1985SoPh...97..345M

SIMULTANEOUS MICROWAVE OBSERVATIONS OF SOLAR FLARES AT 6 AND 20 cm WAVELENGTHS USING THE VLA

M. MELOZZI, M. R. KUNDU, and R. K. SHEVGAONKAR*

Astronomy Program, University of Maryland, College Park, MD 20742, U.S.A.

(Received 2 November, 1984; in final form 26 April, 1985)

Abstract. Using the Very Large Array, solar burst observations have been carried out simultaneously at 6 and 20 cm. Structural changes and preheating have been observed in the flaring regions on time scales of minutes to tens of minutes before the onset of the burst impulsive phase. The 6 cm burst sources are located close to the neutral line, or near the legs of a flaring loop. The 20 cm burst sources show complex and extended structures spatially separated from both the preburst emission and the gradual decay phase of the burst. We interpret the observations in terms of a two-component flare model (bulk heating as well as acceleration of particles) and derive the physical parameters of the burst sources.

1. Introduction

Using high spatial resolution instruments like the Very Large Array (VLA), it is possible to locate the flare position within the complex magnetic structure of the active region with a spatial resolution of a few arc seconds. Also, with a time resolution of ~ 10 s, we can study the physical changes in the preflare active region which are ultimately responsible for the flare.

Previous observations (Alissandrakis and Kundu, 1978; Marsh and Hurford, 1980; Lang *et al.* 1982; Willson, 1983; Shevgaonkar and Kundu, 1985) with high spatial resolution indicate that the microwave burst occurs in loop structures located above or close to a photospheric neutral line. Of particular importance are the changes in the polarization structure and the degree of polarization which have been observed in flaring regions on time scales of minutes to tens of minutes before the impulsive phase (Kundu *et al.*, 1982; Willson, 1983). These variations are attributed to the reorientation or emergence of magnetic fields in coronal loops. Kundu *et al.* (1982) and Kundu and Shevgaonkar (1985) have provided observational evidence for evolving magnetic structures interacting with the pre-existing magnetic fields to trigger flares. However, most of the observations in the past were performed at a single wavelength. Due to the complexity of the burst events, single wavelength observations are inadequate to provide detailed information about the physical parameters of the burst sources.

The previous simultaneous dual frequency observations with high spatial resolution (Shevgaonkar and Kundu, 1985; Dulk *et al.*, 1983) were performed at 6 and 2 cm, covering the high frequency side of the microwave burst spectrum. In this paper, we present simultaneous observations of bursts at 6 and 20 cm. Total intensity (I) and circular polarization (V) maps have been produced during the preflare, impulsive and decay phase of the events and are compared with soft X-ray (1–8 Å) data. We present

* On leave of absence from Indian Institute of Astrophysics, Bangalore, India.

Solar Physics **97** (1985) 345–361. 0038–0938/85.15.
© 1985 *by D. Reidel Publishing Company*

© Kluwer Academic Publishers • Provided by the NASA Astrophysics Data System

1985SoPh...97..345M

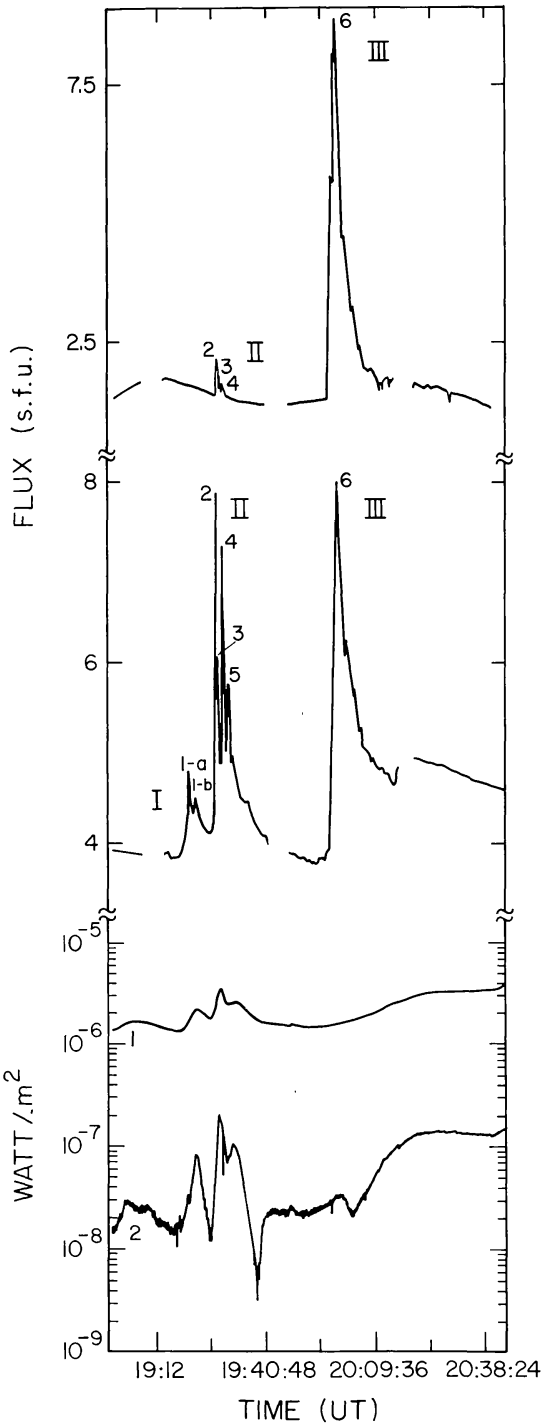

Fig. 1. Time profiles of the fringe amplitude at 20 cm (baseline 1868 λ) (a = top curve) and 6 cm (baseline 1333 λ) (b = middle curve). At the bottom (= c) the soft X-ray emission as recorded by the two GOES channels (1–8 Å upper, 0.5–4 Å lower) is shown.

evidence for the two-component flare model (bulk heating of the plasma as well as acceleration of the particles) as suggested by Böhme *et al.* (1977) from X-ray observations and additionally supported by Shevgaonkar and Kundu (1985) and Dulk *et al.* (1983) using microwave data. Our results indicate that the microwave emission at the longer wavelenght is more susceptible to preflare changes in the active region. Evidence

© Kluwer Academic Publishers • Provided by the NASA Astrophysics Data System

1985SoPh...97..345M

for magnetic structure interaction as a triggering mechanism is presented. From the brightness temperature and degree of polarization at the two wavelengths, physical parameters such as the magnetic field, density, etc. in the flaring region are estimated.

2. Observations

Several bursts occurring in the Hale region 17992 (N 18 W 33 at 00:00 UT) were observed simultaneously at 6 and 20 cm on November 14, 1981 using the Very Large Array (VLA).

During our observations, the VLA was in the C configuration and the 27 antennas were divided into two sub-arrays to provide similar *u-v* coverage at the two wavelengths λ, 6 and 20 cm. The *u-v* coverage for each subarray ranged from $\sim 1000\,\lambda$ to $13\,000\,\lambda$. The visibility data were recorded with the minimum available integration time of 10 s. We have produced two dimensional intensity (I) and circular polarization (V) maps to study the time evolution of the active region radio emission during the period 19:00 to 21:30 UT. The visibility data for time intervals ranging from 15 min to 10 s were used to produce snapshot maps, depending upon how fast the observed flux varied at a certain time. All maps were cleaned using the standard CLEAN technique and the cleaned maps were convolved with a beam $13'' \times 13''$ and $20'' \times 20''$ at 6 and 20 cm, respectively.

Figures 1a, 1b show the total intensity time profiles of the bursts at 20 and 6 cm for the baselines $1868\,\lambda$ and $1333\,\lambda$, respectively. In Figure 1c the soft X-ray (1–8 Å) data recorded by GOES satellite are shown (data provided by B. Dennis). A comparison of the time profiles of the bursts at 6 and 20 cm exhibits the following characteristics.

(1) The peaks at 6 cm indicated by numbers I–1a, I–1b, and II–5 have no detectable peaks at 20 cm.

(2) The radio and soft X-ray impulsive flares for bursts I–1a and II–2 start at the same time ($\pm$ 5 s); the microwaves peak during the soft X-ray gradual phase. The peak I-1b, however, occurs simultaneously with the soft X-ray first maximum.

(3) The peaks II–2, II–3, II–4, and III–6 are temporally correlated at 6 and 20 cm. However time delays of 10–30 s between the burst peaks at the two wavelegths are observed. The time delay does not occur in the same direction.

(4) Even with the low time resolution available with the VLA, it is possible to see structure in the 20 cm time profile of the burst III. However, the 6 cm rise phase does not show a spiky profile.

3. Bursts I and II

3.1. Preflare activity and impulsive phase of burst I

Figure 2a shows a preflare map at 6 cm, produced 25–30 min (19:00 UT) before the impulsive onset of the burst I–1. North is up and west is on the right of the figure. The

© Kluwer Academic Publishers • Provided by the NASA Astrophysics Data System

1985SoPh...97..345M

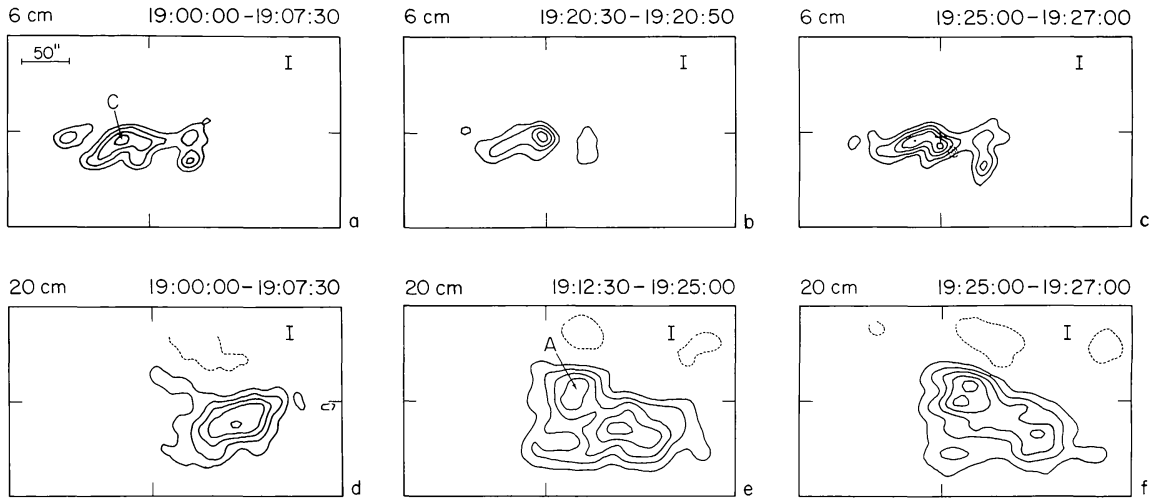

Fig. 2. Sequence of snapshot maps of total intensity (I) at 6 cm (a, b, c) and at 20 cm (d, e, f); (a) map of preburst phase; (b) map of peak I–1a; (c) map in between the bursts I and II. The lowest contour for the 6 cm map is 6.5×10^5 K for the maps (a) and (c) and 1.4×10^6 K for map (b); it is 2×10^5 K for the 20 cm map (d) and 3.1×10^5 K for the maps (e) and (f). The contour intervals are the same as the lowest contours.

total intensity (I) map is elongated in the east–west direction and the source is closely associated with sunspots. Its peak brightness temperature (T_b) is $\sim 2.6 \times 10^6$ K, and it located above a group of small sunspots with magnetic field of negative polarity (the source C in Figure 2a). The degree of polarization is below the instrumental detection limit ($\sim 10\%$). Henceforth, the V-maps are not presented when the degree of polarization is $\leq 15\%$.

The 6 cm emission does not seem to show any significant structural or intensity changes until 19 : 20 : 10 UT, the time of impulsive onset of the burst I–1 which peaked at 19 : 20 : 40 UT with $T_B \sim 6.1 \times 10^6$ K (Figure 2b). The 6 cm bursts source is located above a neutral line of the KPNO magnetogram (Figure 3).

Figure 2c shows the 6 cm total intensity map during the period in between the bursts I and II (19 : 25–19 : 27 UT). This map appears to be a combination of the post-burst emission of the burst I and the preflare emission of the burst II. In the figure the cross represents the positions of bursts I–1 while the dotted lines indicate the location of the co-spatial peaks II–2, 3, 4. The maximum value of T_b ($\sim 3.3 \times 10^6$ K) during this interval is located somewhere in between the burst sources, $\lesssim 15''$ from either peak. Thus, it seems that the burst position in the post-burst phase has shifted from the impulsive peak.

At 20 cm the time profile shows no detectable flux variation until the impulsive onset (at 19 : 27 : 15 UT) of the burst II. However, the preflare map shown in Figure 2e shows significant variation during the time period 19 : 12 : 30–19 : 25 UT, relative to a map at 19 : 00–19 : 07 : 30 UT (Figure 2d). An intense source (A in Figure 2e) with $T_b \sim 1.2 \times 10^6$ K, emerges several minutes (~ 10–15) before the onset of the burst. It should be noted that an increase in the soft X-ray channels was recorded during the time interval $\sim$ 19 : 04 to 19 : 15 UT. Unfortunately a precise relation between the 20 cm and soft X-ray evolution can not be established since the VLA was pointed at the calibrator

© Kluwer Academic Publishers • Provided by the NASA Astrophysics Data System

1985SoPh...97..345M

Fig. 3. KPNO magnetogram November 14. The ovals and the crosses indicate the positions of bursts I, II, III; the box represents the same frame as the VLA maps.

from 19:07:30 to 19:12 UT and we do not have spatially resolved soft X-ray data. Finally a second strong source emerges in the northern part of the 20 cm preflare source with $T_b \sim 1.7 \times 10^6$ K in the time period 19:25–19:27 UT (Figure 2f).

3.2. Impulsive phase of burst II

Since the location and shape of the burst source do not vary during the peaks II–2, 3, and 4, only 10 s maps for the burst peak II–2 are presented in Figures 4a and 4b (6 and 20 cm, respectively). The 6 cm T_b at the peaks II–2, 3, and 4 are $\sim 19.5 \times 10^6$ K, 10×10^6 K, and 19.5×10^6 K, respectively. At the times of the peaks, the brightness temperatures at positions away from the burst peak increase from $\sim 3 \times 10^6$ K to ~ 4.5–6×10^6 K, indicating an interaction between distant burst sources, possibly by some kind of magnetic loop structure linking the two regions (see in particular at the position of source *C*). The 6 cm peak II–5 (Figure 4e), which is not detected at 20 cm, has a slightly different location; this burst source is displaced by $\sim 16''$ (HPBW = $13''$) in the north–east direction relative to the previous peaks. The T_b in this case is $\sim 7.3 \times 10^6$ K.

Figure 4b shows the 10 s 20 cm map at the time of the peak II–2. The burst source position seems displaced to the north–east by $\sim 20''$–$25''$ relative to the 6 cm peak position (dashed lines). It should be noted, however, that the displacement is of the same

© Kluwer Academic Publishers • Provided by the NASA Astrophysics Data System

1985SoPh...97..345M

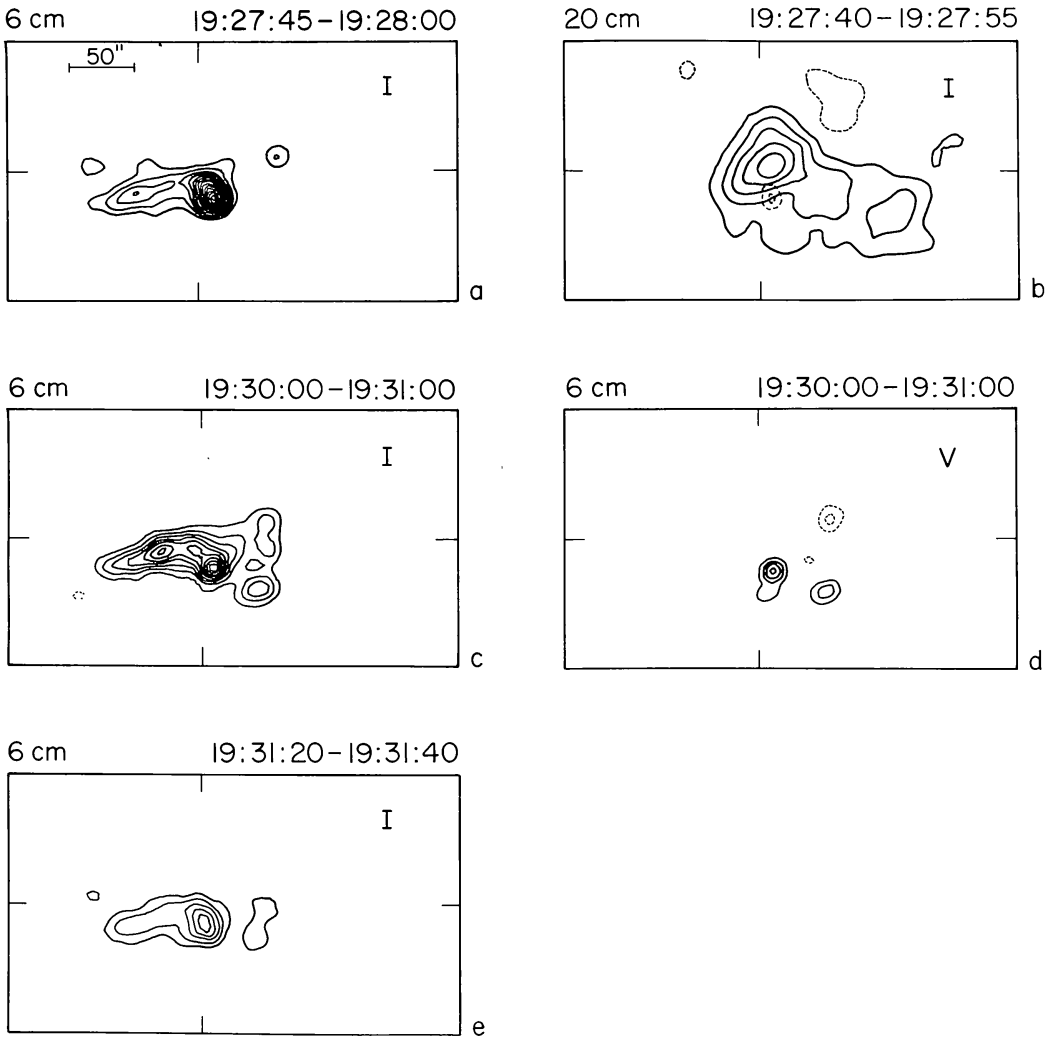

Fig. 4. Snapshot maps for burst II. (a) 6 cm I-map of peak II–2; (b) 20 cm I-map of peak II–2. (c) and (d) are the 6 cm I-map and V-map in between peaks II–4 and II–5, respectively; (e) 6 cm I-map of peak II–5. The lowest contour level is 1.3×10^6 K for Figures 3(a) and 3(e); it is 6.2×10^5 K for Figure 3(b) and 6.5×10^5 K and 3.25×10^5 K for 3(c) and 3(d), respectively. In the 20 cm map (Figure 3b) the dashed line represents the position of the burst at 6 cm. The uncertainties in the relative position is determined by the HPBW. In the V-map right and left circular polarization are represented by solid and dashed contours. The contour intervals are the same as the lowest contours.

order as the 20 cm HPBW (20″). The brightness temperatures around the 20 cm peaks are $T_b \sim 3.6 \times 10^6$ K, 3.5×10^6 K, and 2.95×10^6 K, respectively. The degree of polarization during the burst peaks is $\lesssim 10\%$ at both wavelengths. However, the 6 cm I and V maps (Figures 4c and 4d), produced during the decay phase of the peak II–4 show an increase of the degree of polarization to $\sim 23\%$.

Figure 5a shows a 15 min (19 : 35–19 : 50 UT) map at 6 cm after the last peak of the burst II. In addition to the source *C* that exists in the preflare map of Figure 2a, a new source *E* appears in the map. The source *E* is cospatial with the position of burst peak II–5 and its emission probably corresponds to the gradually declining post-burst phase of this burst. The T_b of the source *C* is $\sim 3.2 \times 10^6$ K, somewhat higher than the preburst brightness temperature. The intensity of the source *E* gradually decreases and by

© Kluwer Academic Publishers • Provided by the NASA Astrophysics Data System

1985SoPh...97..345M

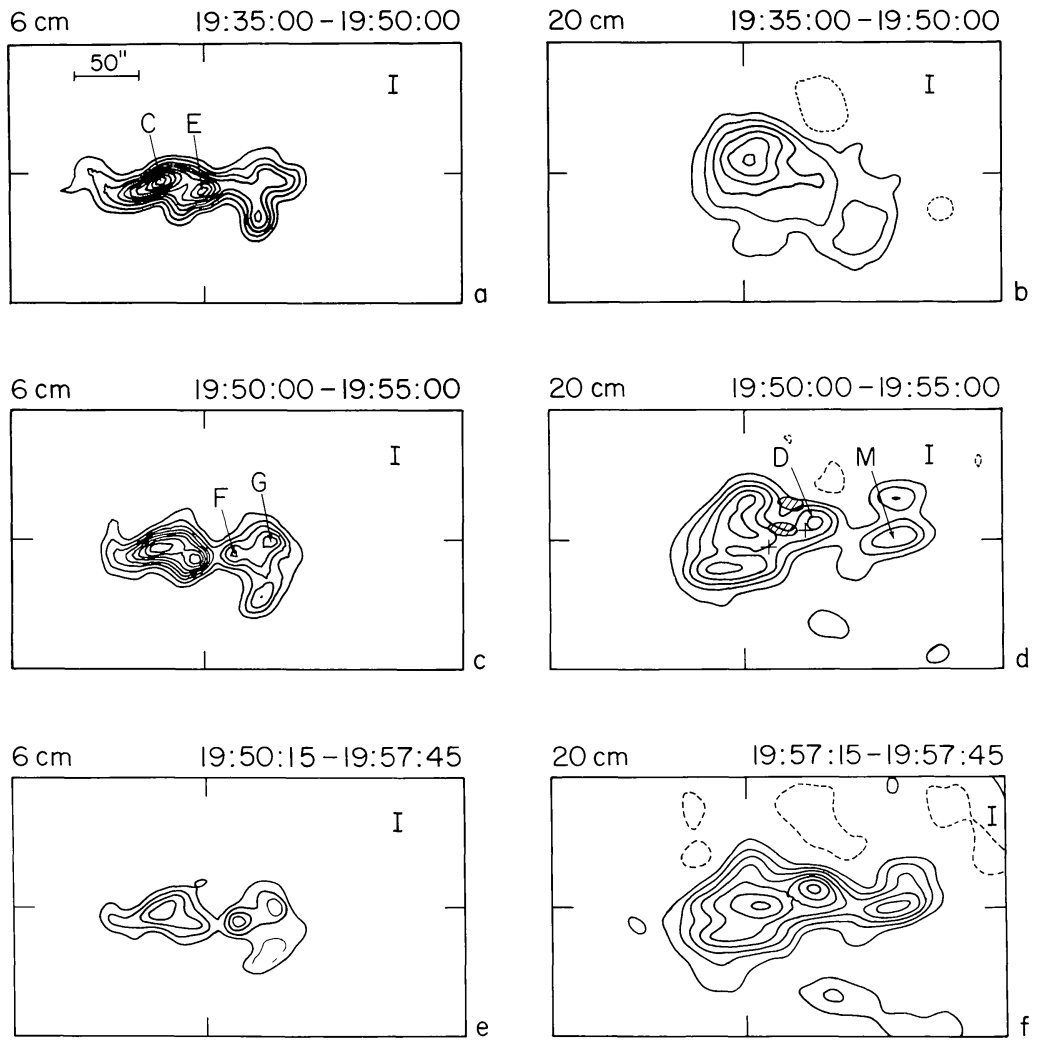

Fig. 5. Snapshot maps during the time interval in between bursts II and III. (a) and (b) are 15-min maps at 6 cm and 20 cm (19 : 35–19 : 50 UT); (c) and (d) are 5-min maps at 6 cm and 20 cm; (e) and (f) are 30 s maps at 6 and 20 cm. The lowest contour level is 3.25×10^5 K for the 6 cm maps (a) and (c), and 6.5×10^5 K for map (e); it is 3.1×10^5 K for the 20 cm maps. The contour interval is the same as the lowest contour.

19 : 56 UT the radio brightness in the westermost part comes to its preburst level.

A 15 min map at 20 cm during the post-burst phase (19 : 35–19 : 50 UT) shows that the total intensity distribution changes relative to its preburst structure (see Figures 2e and 5b). As one can see from Figure 5b, in the post-burst phase the T_b remains high ($\sim 1.9 \times 10^6$ K) at the position where the burst occurred, whereas in the southernmost part of the source, the T_b is considerably reduced ($T_b \lesssim 6 \times 10^5$ K).

3.3. Burst III

3.3.1. *Preflare Activity*

Two new sources, *F* and *G*, appeared 5–10 min before the onset of the impulse phase (see Figure 5c), which is indicative of preflare activity related to the burst peak III–6; the brightness temperature is $\sim 1.6 \times 10^6$ K for both the sources.

© Kluwer Academic Publishers • Provided by the NASA Astrophysics Data System

1985SoPh...97..345M

Figure 5d shows a 5-min (19 : 50–19 : 55 UT) map at 20 cm, ~5–10 min before the onset of the burst III. Two more sources, *D* and *M*, with $T_b \sim 1.4 \times 10^6$ K and 1.1×10^6 K respectively are present in the map. In Figure 5d the shaded areas represent the position of the 20 cm burst sources *H* and *K* at the time of the peak (cf. Figure 7b). The crosses indicate the position of the 6 cm sources *F* and *G*. The morphology of the preflare brightness distribution remains the same until the onset of the impulsive phase at ~19 : 57 : 45 UT. On the other hand, the T_b of the sources increases with time. Just before the impulsive phase onset, *F* and *G* have $T_b \sim 3 \times 10^6$ K and 2.3×10^6 K respectively while the source *D* has $T_b \sim 2.8 \times 10^6$ K (Figures 5e and 5f).

3.3.2. *Impulsive Phase*

Figure 6a shows a 30-s total intensity map at the very beginning of the impulsive rise phase of the burst III at 6 cm. Figures 6b and 6c show the corresponding 20 cm total intensity and circular polarization maps. At 6 cm the burst radiation originates from two strong sources (the sources *F* and *G* previously referred to) with $T_b \sim 6 \times 10^6$ K and 9.5×10^6 K, respectively.

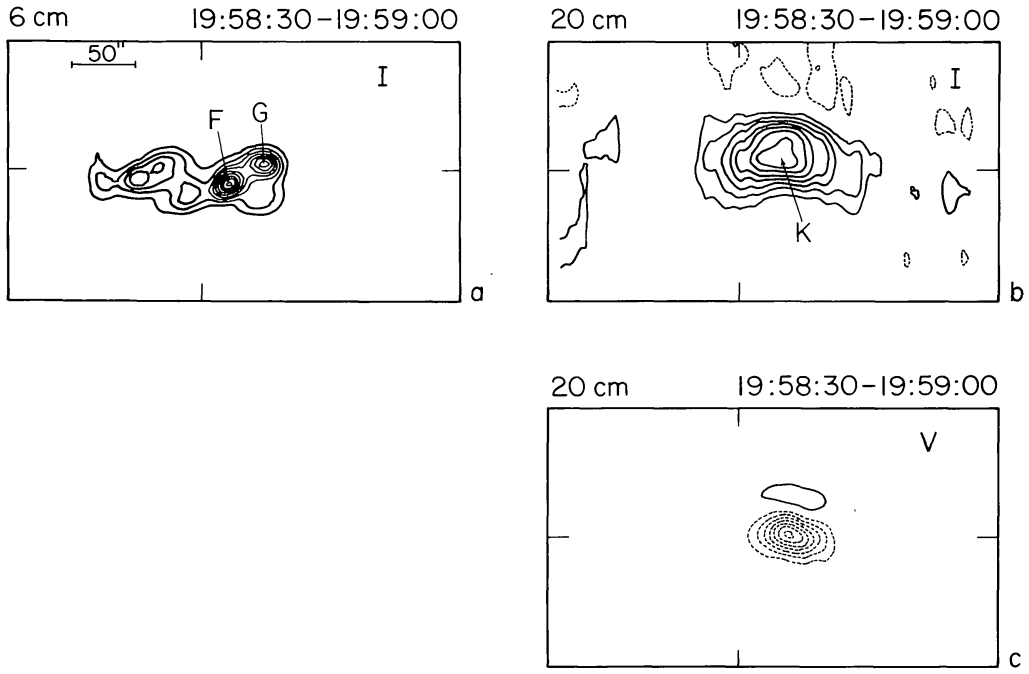

Fig. 6. Snapshot maps at the beginning of the impulsive phase of burst III. The lowest contour level for the 6 cm I-map is 6.5×10^5 K (a); it is 10^6 K for the 20 cm I-map (b) and 4.1×10^5 K for the 20 cm V-map (c). Right and left circular polarization are represented by solid and dashed lines.

At 20 cm the peak T_b is 7.8×10^6 K (the *K* in Figure 6b) and the source exhibits a bipolar structure, one component being more strongly polarized than the other. The maximum degree of polarization is ~40%.

The 10-s maps at the peak of the impulsive phase of burst III are shown in Figures 7a,

© Kluwer Academic Publishers • Provided by the NASA Astrophysics Data System

1985SoPh...97..345M

7b (6 cm) and 7c, 7d (20 cm). At 6 cm the two peaks F and G have $T_b \sim 11.8 \times 10^6$ K and 8.8×10^6 K, respectively. Only F shows detectable right-handed polarized emission ($\sim 22\%$).

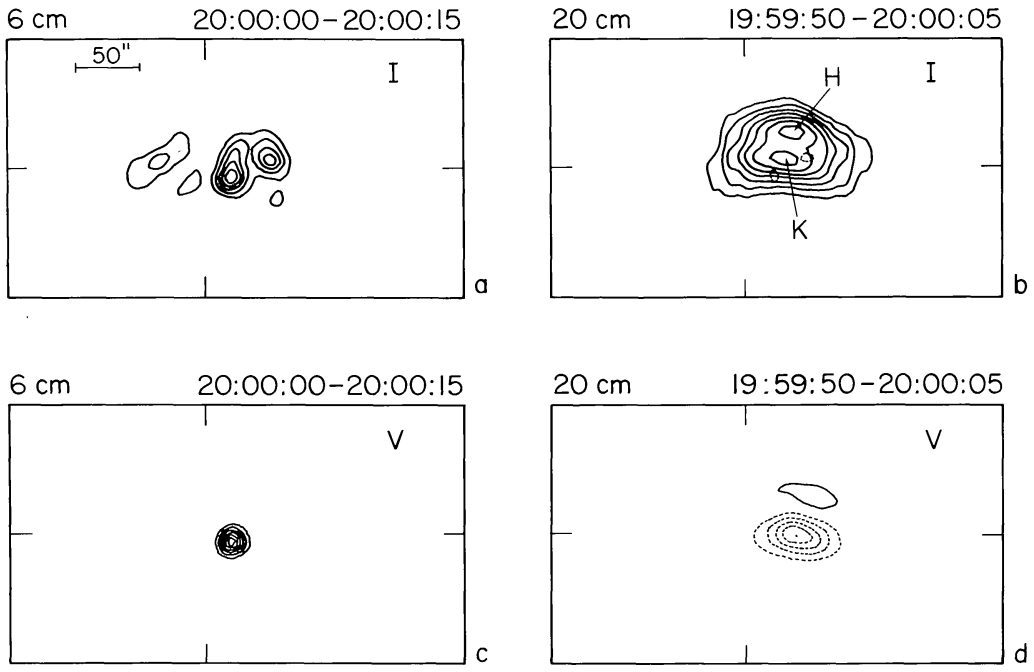

Fig. 7. 10-s snapshot maps at the peak of the impulsive phase of burst III. The lowest contour level is 1.95×10^6 K for the I-map at 6 cm (a); it is 3.1×10^6 K for the I-map at 20 cm (b). For the V-maps the lowest contour level is 4×10^5 K at 6 cm (c) and 2.1×10^6 K at 20 cm (d). The contour interval is the same as the lowest contour. Right and left circular polarization are represented by solid and dashed contours.

Figure 7c shows that at 20 cm a second peak (indicated by H) is also present along with the peak K. The two peaks H and K have approximately equal T_b ($\sim 23 \times 10^6$ K), but opposite senses of polarization. In the regions where 20 and 6 cm sources overlap, the polarized emission at 6 cm is opposite in sense to the 20 cm polarized emission.

Figures 8a and 8b show 6 cm maps during the decay phase of the burst. The peak T_b's of the sources F and G in Figure 8a are 5.3×10^6 K and 4.2×10^6 K, respectively. At 20:30–20:45 UT (Figure 8b) F and G merge into a single source with $T_b \sim 5.1 \times 10^6$ K. The degree of polarization is below the detection limit. After an additional 45–60 min, the burst source evolves to a new configuration characterized by two extended sources (Figure 8c); their peak T_b's are 2.2×10^6 K and 3.1×10^6 K, respectively.

Figures 8d and 8e show the 20 cm I-maps, 15 and 30 min after its peak. The position of the peak T_b ($\sim 3.5 \times 10^6$ K) is cospatial with the source D in Figure 5d. The source seems to broaden with time, without varying significantly in intensity. Figure 8f shows the 20 cm I-map at $\sim$21:15 UT. The peak T_b is 1.9×10^6 K.

Our main results can be summarized as follows:

© Kluwer Academic Publishers • Provided by the NASA Astrophysics Data System

1985SoPh...97..345M

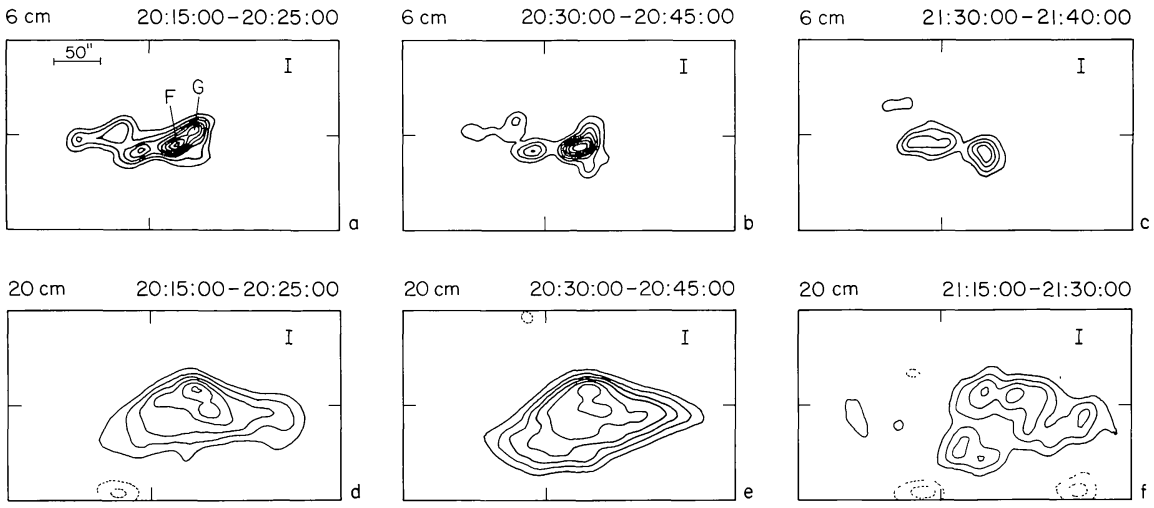

Fig. 8. Sequence of snapshot maps after the peak of burst III. The 6 cm maps (a), (b), and (c) are produced over the time intervals 20 : 15–20 : 25 UT, 20 : 30–20 : 45 UT, 21 : 30–21 : 40 UT, respectively; (d), (e), and (f) are 20 cm maps during the time intervals 20 : 15–20 : 25 UT; 20 : 30–20 : 45 UT; and 21 : 15–21 : 30 UT, respectively. The lowest contour level is 6.5×10^5 K for the 6 cm maps; it is 5.2×10^5 K for the 20 cm maps. The contour interval is the same as the lowest contour.

(1) The 20 cm emission varies significantly before the onset of the flare. Physical changes take place in the preflare active region, 10–15 min before the onset of the impulsive phase. During the decay phase, a different source structure develops, relative to the preburst phase. At 6 cm for the burst I, and II a distinct precursor phase is not observed. However for the burst III, the intensity starts to rise $\sim$4–6 min before the onset of the impulsive phase.

(2) The impulsive phase for bursts I and II starts simultaneously with the rising phase in soft X-ray and in the case of peak I–1b the emission peaks simultaneously in both X-rays and microwaves. The peaks in bursts I and II are rather weakly polarized ($\leq 15\%$) and the peak brightness temperatures at 6 cm for burst II are higher than those at 20 cm. The burst III shows significant polarization at both wavelengths and T_b at 20 cm is higher than at 6 cm. For bursts I and II–5, the impulsive phase at 20 cm was not detected.

4. Discussion

4.1. Preflare activity

The large variations in radio emission observed before the burst onset are obviously related to the flare build-up process. The variations in 20 cm emission are observed $\sim$15 min before the onset of the peak II–2. Similar results have been reported by Willson and Lang (1984). The appearance of new microwave sources during the preflare phase could be either due to a change in the parameters of the ambient thermal plasma or due to the acceleration of electrons to mildly relativistic energies.

© Kluwer Academic Publishers • Provided by the NASA Astrophysics Data System

1985SoPh...97..345M

Since the preburst emission for all the observed bursts is unpolarized the former possibility seems more likely. The cause of the brightness temperature increase is not clear. Various authors (e.g. Heyvaerts *et al.*, 1977; Spicer, 1977) in the course of proposing different flare models have suggested that a part of energy released during the flare build-up goes into heating of the plasma. For example, considering an emerging flux flare model, and assuming that the heat to the surrounding plasma is released by shock waves emanating from the current sheet, Heyvaerts *et al.* (1977) inferred an energy release rate of $\sim 8 \times 10^{25}$ ergs s^{-1}. For our observations, assuming a source height of $\sim 10^9$ cm and neglecting the radiation losses, the rate of increase of the thermal energy necessary to obtain the observed brightness is in the range 10^{25}–2×10^{26} ergs s^{-1}.

Along with the heating of the plasma, other factors could determine the development of new microwave regions. For example, as suggested by Kundu *et al.* (1982) the onset of currents in the region can increase the magnetic field strength such that the corona becomes optically thick at low harmonics of the gyrofrequency. It can be shown however that unless we assume an angle θ between the magnetic field and the line of sight, $\geq 60°$, an increase of magnetic field strength is not consistent with the measured values of T_b.

The preburst emission at 6 cm for burst III (sources *F* and *G*) appears to be originating from the legs of a loop whose footpoints are located near two sunspots of opposite polarity. During the preburst phase, the growth in intensity of the two sources *F* and *G* show up simultaneously while the top of the loop does not show any variation until the onset of the impulsive phase. The entire loop is probably heated and the brightening is observed only at those points where the magnetic field is high enough for gyroresonance mechanism to be efficient.

4.2. Impulsive phase

4.2.1. *Bursts I and II*

The 6 cm impulsive phase of bursts I and II starts simultaneously (± 5 s) with the soft X-ray rising phase indicating that at least at the very beginning of the events, part of the energy released goes into heating of the plasma.

The parameters of the plasma can be derived from the ratio of the two soft X-ray channels using the formula of Thomas *et al.* (1984). At the time of 6 cm peak I–1a it turns out that the electron temperature T_e is $\sim 5.5 \times 10^6$ K and the volume emission measure *EM* is $\sim 2 \times 10^{48}$ cm^{-3}. As we shall see later in the discussion of peak I–1b, the magnetic field in the burst source should be ≤ 350 gauss; the contribution of the X-ray plasma to the radio emission is essentially determined by thermal bremsstrahlung. The thermal brightness temperature (assuming T_e = constant) turns out to be $\sim 4 \times 10^6$ K if we assume that the density is a function only of z (the direction along the line of sight) and that the X-ray and radio sources have the same dimension (measured area $\sim 10^{18}$ cm^2). Therefore in addition to the heating of the plasma, there must be acceleration to account for the observed $T_b \sim 6.1 \times 10^6$ K; the contribution of the nonthermal particles to the brightness temperature is $\sim 2 \times 10^6$ K. This can be

© Kluwer Academic Publishers • Provided by the NASA Astrophysics Data System

1985SoPh...97..345M

achieved if 10^3–10^4 particles cm^{-3} with energy $\gtrsim 40$ keV, following a power law with exponent $\delta \sim 3$, emit gyrosynchrotron radiation in a dense plasma (if $z \sim 10^9$ cm, the density N_T of the thermal plasma $\approx 4.5 \times 10^{10}$ cm^{-3}) with magnetic field ~ 200–350 gauss. For the above computations we have assumed that the angle, θ, between the magnetic field and the direction of the observer, is $\sim 75°$. (This seems to be a reasonable assumption since the 6 cm emission is observed close to a magnetic neutral line implying its origin from the top of a loop.) The degree of polarization, p, of the radio source is below the detection limit; the value of p due to mildly relativistic particles in the presence of a thermal plasma is lowered by a factor

$$1 + \frac{T_{bT}}{T_{bnT}} \simeq 3 , \tag{1}$$

where T_{bT} and T_{bnT} refer to the thermal and nonthermal contribution to the total brightness temperature.

The 6 cm emission peaks a second time with $T_B \sim 4$–4.5×10^6 K simultaneously with the soft X-ray emission, indicating the thermal origin of the burst radiation. In this case the soft X-ray emission indicates that $T_e \sim 8.4 \times 10^6$ and $EM \sim 2 \times 10^{48}$ cm^{-3}. The 6 cm T_b is less than the actual electron temperature, and the plasma should be optically thin. Therefore we can rule out any substantial contribution of gyroresonance absorption to the radio opacity and the magnetic field in the source should be < 350 gauss as previously indicated. The emission should be due to thermal bremstrahlung; in this case the brightness temperature turns out to be 4.1×10^6 K in substantial agreement with the observations.

The 6 cm burst for the peaks II–2, 3, and 4 are cospatial; however they are displaced by $\sim 20''$ with respect to the burst peak I–1. Since the displacement is in the southwest direction, it is not due to a difference in height. Therefore it seems that different loops may be involved in producing bursts at different wavelengths. As in the previous case, the 6 cm emission peaks impulsively, superposed on the gradual heating of the burst source (as evidenced by the soft X-ray emission).

The emission during the impulsive phase is due to energetic electrons emitting gyrosynchrotron radiation. The soft X-ray data indicate that $T \sim 6.7$–7.4×10^6 K and $EM \sim 4$–5×10^{48} cm^{-3}. For such value of EM, impulsive heating to $\sim 20 \times 10^6$ K should manifest itself in the GOES channels. Since no impulsive soft X-rays are observed simultaneously with the radio peaks, the electron energy distribution must be nonthermal. If the sizes of the soft X-ray and radio sources are similar (and assuming $z \sim 10^9$ cm), the density of the thermal plasma is ~ 6–8×10^{10} cm^{-3}. The high density of the source is confirmed also by the spectrum of the event. Indeed, the spectrum of the peak II–2 has a U-shaped signature with a cut-off frequency at $\sim 2.5 \times 10^9$ Hz (*Solar Geophysical Data*). Assuming this frequency to be equal to the plasma frequency of the source (Kundu and Vlahos, 1982), a density of 8×10^{10} cm^{-3} is estimated, which is consistent with the soft X-ray measurements. The brightness temperature ($T_b = T_{b+} + T_{b-}$ where + and − refer to the o-mode and x-mode, respectively) and

© Kluwer Academic Publishers • Provided by the NASA Astrophysics Data System

1985SoPh...97..345M

the degree of polarization p for a plasma volume consisting of thermal and nonthermal particles, with the temperature $T \simeq 7 \times 10^6$ K and density $N_T \approx 8 \times 10^{10}$ cm^{-3} for the thermal plasma, can be computed by solving the equation of transfer (see e.g. Chiuderi–Drago and Melozzi, 1984). Since the degree of polarization is $< 10\%$ at the maximum of the burst, and it increases when the intensity decreases, the emission at the peak of the impulsive phase is optically thick and, the brightness temperature should be $\gtrsim 10^8$ K. Therefore the observed value of T_b ($\sim 20 \times 10^6$ K) requires an absorption by the overlying layer of the atmosphere. The optical depth τ_u of the absorbing layer should be ~ 2–2.5 giving a density above the burst source of $\sim 2 \times 10^{10}$ cm^{-3} if the temperature of the layer is $\sim 2 \times 10^6$ K. Assuming the source to be isothermal and a power-law distribution with $\delta = 3$ and 4 for the accelerated electrons (density N_R), the brightness temperature and the degree of polarization after the absorption by the upper layer, are plotted against the magnetic field in Figures 9a and 9b, respectively. As can be seen the radiative characteristic of the burst source at 6 cm can be fitted by: $350 \lesssim B \lesssim 600$ gauss, $N_R \sim 10^5$–10^6 cm^{-3}, $\delta \sim 3$–4 with $N_T \sim 8 \times 10^{10}$ cm^{-3}. The higher polarization in between the peaks III–4 and III–5 indicates that the source evolves toward an optically thin status during the decay phase. After the impulsive peak, the number of accelerated particles decreases ($\leq 10^5$ cm^{-3}), along with the value of the exponent of the power-law distribution; the source becomes optically thin and the polarization increases.

The absence of radiation signature at longer wavelengths during multifrequency observations of flares has also been reported by Shevgaonkar and Kundu (1985) and Dulk *et al.* (1983). Shevgaonkar and Kundu have argued that the absence of low frequency emission is due to the intrinsic nature of the burst source, whereas Dulk *et al.* have suggested that this effect may be due to absorption of the burst emission by the higher optically thick layers of the active region atmosphere.

Takakura (1959) suggested that the low frequency emission does not escape from the burst source since it is lower than the critical frequencies,

$$\nu_p \quad \text{and} \quad \frac{\nu_B}{2} + \left(\frac{\nu_B^2}{4} + \nu_p^2\right)^{1/2}$$

(ν_p and ν_B are the plasma frequency and gyrofrequency) for the ordinary and extra-ordinary modes, respectively. It follows from the previous discussion that the density of the microwave source ranges between 3×10^{10} cm^{-3} and 8×10^{10} cm^{-3}. Therefore the high density of the source could be responsible for the attenuation of the 20 cm emission. However we can not rule out the effect of gyroresonance absorption by the upper layer of the atmosphere ($B \sim 170$ gauss). Since in the case of bursts I and II–5 at 20 cm there is no detectable impulsive emission, we believe that the accelerated particles can not escape from the 6 cm burst site toward lower density region. For peaks II–2, 3, and 4 the 20 cm emission may not be directly associated with the 6 cm source. Also the slight displacement of 20 cm burst relative to the 6 cm source may imply that the 20 cm emission occurs in a different loop or at a different height in the same magnetic arcade; both burst sources are probably magnetically connected.

© Kluwer Academic Publishers • Provided by the NASA Astrophysics Data System

1985SoPh...97..345M

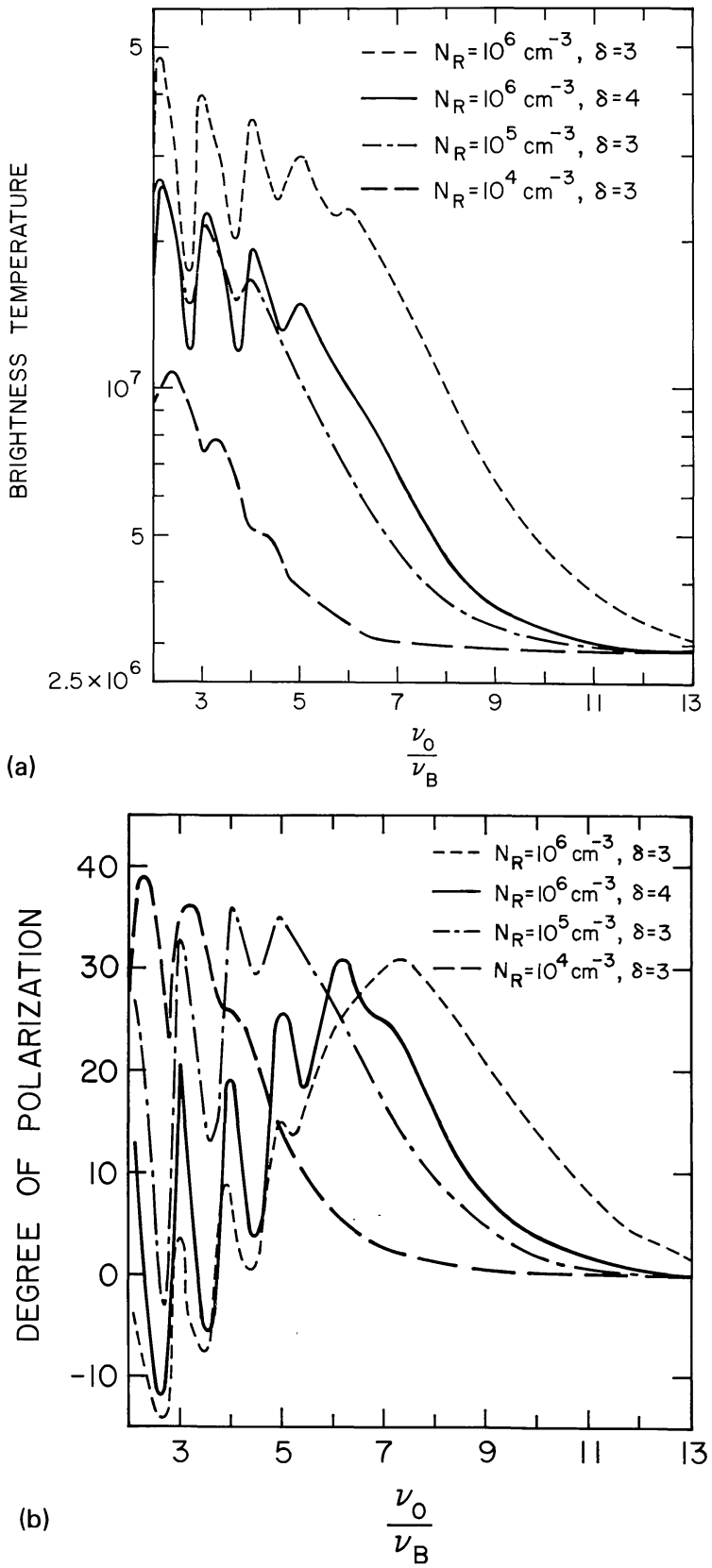

Fig. 9. (a) Brightness temperature T_b and (b) degree of polarization as a function of magnetic field, due to synchroton radiation from energetic electrons with a power-law distribution (exponent δ and low energy cutoff E = 40 keV) inside a plasma volume with ambient density $N_T \simeq 8 \times 10^{10}$ cm^{-3} and temperature $T \simeq 7 \times 10^6$ K. The angle θ between the line of sight and the magnetic field is 75°. Thermal absorption by an overlying layer is assumed (optical depth $\tau_u \approx 2.3$; $\nu_0 = 5$ GHz).

© Kluwer Academic Publishers • Provided by the NASA Astrophysics Data System

1985SoPh...97..345M

4.2.2. *Burst III*

The spike-like structure in the 20 cm burst time profile could be due to the long integration of multiple short lived bursts. Indeed, the fact that a new source K emerges ~ 1 min after the beginning of the impulsive phase in the northernmost part of the source, implies that energy release location changes with time.

At the onset of the impulsive phase, the 6 cm emission arises from a magnetic loop which is similar in structure and is cospatial with the loop responsible for the preflare emission. However the 20 cm source exhibits a complex and large magnetic structure, which is not visible during the preburst phase.

The burst source at the peak of the impulsive phase consists of two loops (F and G at 6 cm, and K and H at 20 cm) which as a whole resemble a quadrupole structure. The lack of polarized emission from the source G could probably be due to the magnetic asymmetry of the loop emitting 6 cm radiation (Kundu and Vlahos, 1979).

Since the radiation at the two wavelengths originates from different magnetic structures, different senses of polarization at 6 and 20 cm can not be referred to as 'polarization reversal'. It is worth noting that such a conclusion could be arrived at only from high spatial resolution observations such as are available with the VLA.

Assuming that the electrons follow a power law distribution with average exponent $\delta = 3$, the lack of 6 cm emission in the 20 cm source gives an upper limit of 100 gauss for the magnetic field. Indeed, the observations are consistent with $N_R \approx 10^5$, $50 \leq B \leq 80$ gauss and $\theta \sim 60°$. The different degrees of polarization in the sources K and H must be due to different values of the angle θ between the line of sight and the magnetic field; in particular θ has to be closer to 90° for the northern source H.

If the nonthermal particles penetrate through the high magnetic field in the legs of the loop where θ is $\sim 45°$–$60°$, the emission at 6 cm due to the gyrosynchroton radiation of these particles would be highly polarized. Therefore the observed low values of polarization can only be explained if the contribution to the total emission of the unpolarized thermal component is dominant over the nonthermal one. According to Equation (1), the observed degree of polarization indicates that $T_{bT} \gtrsim 2.5\, T_{bNT}$ where T_{bT} and T_{bNT} are thermal and nonthermal brightness temperatures ($T_{bT} + T_{bNT} = T_b$). The volume emission measure from the soft X-ray data is $\sim 1.7 \times 10^{47}\ \mathrm{cm}^{-3}$ and $T_e \sim 10 \times 10^6$ K. If we assume the density to be a function only of z, $\int N^2\, \mathrm{d}z \sim 4.2 \times 10^{28}$ (measured area $\sim 4 \times 10^{18}\ \mathrm{cm}^2$). Therefore the plasma is optically thin for free-free ($\tau \sim 10^{-2}$) and the emission mechanism should be gyroresonance. If z is taken $\sim 10^9$ cm, the average density in the source is $\sim 6 \times 10^9\ \mathrm{cm}^{-3}$. The highest harmonic which becomes optically thick in both ordinary and extraordinary mode is the fourth giving a lower limit for the magnetic field in the loop of ~ 450 G.

4.2.3. *Post Burst*

In the case of burst III the evolution of the 6 cm source after the impulsive phase can be explained by assuming that the density increases toward the loop top, possibly by chromospheric evaporation. The energy of the particles streaming along the field lines

© Kluwer Academic Publishers • Provided by the NASA Astrophysics Data System

1985SoPh...97..345M

is deposited in the low atmosphere and goes into heating of the plasma. The heated plasma expands along the magnetic field lines to form a hot and dense region in the corona. The soft X-ray emission measure increases with time from 1.7×10^{47} cm^{-3} at 20:00:00 to 4×10^{48} cm^{-3} at 20:25:00. As the plasma fills the loop emitting 6 cm radiation, the sources *F* and *G* gradually merge into a single source at the top of the loop. The soft X-ray data indicate an average temperature of ~ 7–8×10^6 K. Assuming the density to be only a function of height, from the measured area (1.5×10^{18} cm^2) we can compute the value of $\int N^2 \, dz \sim 2.4 \times 10^{30}$ cm^{-5}. The free-free contribution of the plasma to the radio emission is $T_b = T_e(1 - e^{-\tau}) \sim 5 \times 10^6$ K consistent with the observed brightness.

At 20 cm due to the weak magnetic field and low electron density during the decay phase, the burst source is not located in the same position as the impulsive phase. The 20 cm source at this time appears to be restored to its preburst position. The fine structures seen in the 20 cm map at 21:15 UT are probably due to the preflare buildup of a region responsible for a large flare that peaked at $\sim$22:00 UT.

5. Summary and Conclusions

In this paper we have presented the spatial properties of several microwave burst sources during the preburst, impulsive and gradual phases of their evolution. Our findings can be summarized as follows.

(1) At 20 cm, preburst heating (10^{25}–10^{26} ergs s^{-1}) and structural changes were observed on time scales of several minutes before the onset of the impulsive phase. For bursts I and II it was not possible to find a clear precursor phase at 6 cm; however, for the burst III enhanced emission was observed from the legs of a quiescent loop as an indication of preburst heating, a few minutes before the onset of the impulsive phase.

(2) Comparison between soft X-ray and 6 cm data indicates that at least at the beginning of the impulsive phase the energy goes into heating of the plasma. The energy is converted into heating even after acceleration of particles occurs (burst I). The displacement of the 20 cm impulsive source relative to the 6 cm source indicates that the 20 cm emission occurs in a different loop or at a different height within the same magnetic arcade; the 20 cm burst source may be somehow linked with the 6 cm burst source.

(3) For burst III, it appears that a two component flare model, namely the acceleration of particles along with bulk heating of the plasma is needed to explain the observations satisfactorily. The synthesized maps of the burst source suggests that the energy release occurs in two different loops. We can speculate that the impulsive phase of the burst is probably triggered by the interaction of a quiescent loop which is observed during the preflare phase ($B \geq 450$ gauss, $EM \lesssim 2 \times 10^{47}$ cm^{-3}) with an overlying magnetic structure. After the burst the evolution of the 6 cm source and the increase of soft X-ray emission measure by more than one order of magnitude may suggest chromospheric evaporation. During this phase thermal free-free emission can account for the observed brightness temperature.

© Kluwer Academic Publishers • Provided by the NASA Astrophysics Data System

1985SoPh...97..345M

Acknowledgements

The Very Large Array is operated by the National Radio Astronomy Observatory under contract with the National Science Foundation. This research was supported by NSF grant ATM 84–15388 and NASA grant NGR 21–002–199. M. M. acknowledges an IAU travel grant. We thank F. Chiuderi Drago for helpful comments.

References

Alissandrakis, C. E. and Kundu, M. R.: 1978, *Astrophys. J.* **222**, 342.
Böhme, A., Fürstenberg, F., Hildebrandt, J., Saal, O., Krüger, A., Hoyng, P., and Stevens, G. A.: 1977, *Solar Phys.* **53**, 139.
Chiuderi Drago, F. and Melozzi, M.: 1984, *Astron. Astrophys.* **131**, 103.
Dulk, G. A., Bastian, T. S., and Hurford, G. J.: 1983, *Solar Phys.* **86**, 219.
Heyvaerts, J., Priest, E. R., and Rust, D. M.: 1977, *Astrophys. J.* **256**, 123.
Kundu, M. R.: 1965, *Solar Radio Astronomy*, Interscience, New York.
Kundu, M. R. and Shevgaonkar, R. K.: 1985, *Astrophys. J.* **291**, 860.
Kundu, M. R. and Vlahos, L.: 1979, *Astrophys. J.* **232**, 595.
Kundu, M. R. and Vlahos, L.: 1982, *Space Sci. Rev.* **32**, 405.
Kundu, M. R., Alissandrakis, C. E., and Kahler, S. W.: 1976, *Solar Phys.* **50**, 429.
Kundu, M. R., Schmahl, E. J., Velusamy, T., and Vlahos, L.: 1982, *Astron. Astrophys.* **108**, 188.
Lang, K. R., Willson, R. F., and Felli, M.: 1981, *Astrophys. J.* **247**, 338.
Marsh, K. A. and Hurford, G.: 1978, *Astrophys. J. Letters* **240**, L111.
Rust, D. M. and Somov, B. V.: 1984, *Solar Phys.* **93**, 95.
Shevgaonkar, R. K. and Kundu, M. R.: 1985, *Astrophys J.* **292**, 733.
Spicer, D. S.: 1977, *Solar Phys.* **53**, 305.
Takakura, T.: 1959 in R. N. Bracewell (ed.), *Paris Symp. on Radio Astronomy*, p. 262, Stanford Univ. Press.
Thomas, R. J., Starr, R., and Crannell, C. J.: 1984, NASA, Technical Memorandum 86142.
Velusamy, T. and Kundu, M. R.: 1982, *Astrophys. J.* **258**, 388.
Willson, R. F.: 1983, *Solar Phys.* **83**, 285.
Willson, R. F. and Lang, K. R.: 1984, *Astrophys. J.* **279**, 427.

© Kluwer Academic Publishers • Provided by the NASA Astrophysics Data System